AIP | The Journal of Chemical Physics

Focus Article: Theoretical aspects of vapor/gas nucleation at structured surfaces

Simone Meloni, Alberto Giacomello, and Carlo Massimo Casciola

Citation: The Journal of Chemical Physics **145**, 211802 (2016); doi: 10.1063/1.4964395
View online: http://dx.doi.org/10.1063/1.4964395
View Table of Contents: http://scitation.aip.org/content/aip/journal/jcp/145/21?ver=pdfcov
Published by the AIP Publishing

Focus Article: Theoretical aspects of vapor/gas nucleation at structured surfaces

Simone Meloni,[a] Alberto Giacomello,[b] and Carlo Massimo Casciola
Department of Mechanical and Aerospace Engineering, Sapienza University of Rome, via Eudossiana 18, 00184 Roma, Italy

(Received 30 June 2016; accepted 24 September 2016; published online 24 October 2016)

Heterogeneous nucleation is the preferential means of formation of a new phase. Gas and vapor nucleation in fluids under confinement or at textured surfaces is central for many phenomena of technological relevance, such as bubble release, cavitation, and biological growth. Understanding and developing quantitative models for nucleation is the key to control how bubbles are formed and to exploit them in technological applications. An example is the *in silico* design of textured surfaces or particles with tailored nucleation properties. However, despite the fact that gas/vapor nucleation has been investigated for more than one century, many aspects still remain unclear and a quantitative theory is still lacking; this is especially true for heterogeneous systems with nanoscale corrugations, for which experiments are difficult. The objective of this focus article is analyzing the main results of the last 10-20 years in the field, selecting few representative works out of this impressive body of the literature, and highlighting the open theoretical questions. We start by introducing classical theories of nucleation in homogeneous and in simple heterogeneous systems and then discuss their extension to complex heterogeneous cases. Then we describe results from recent theories and computer simulations aimed at overcoming the limitations of the simpler theories by considering explicitly the diffuse nature of the interfaces, atomistic, kinetic, and inertial effects. [http://dx.doi.org/10.1063/1.4964395]

I. INTRODUCTION

The formation and evolution of vapor and gas bubbles in a liquid body is a phenomenon of vast fundamental and applicative interest. Bubble nucleation can be exploited for heat transfer,[1] which is at the basis of sonochemistry,[2] while the implosion of bubbles (cavitation) can induce significant damage in submerged parts (e.g., propeller blades).[3]

Nucleation in liquids is greatly enhanced by the presence of impurities, both at submerged surfaces or in the form of advected particles.[4] Solids are typically characterized by surface roughness with a complex, irregular topography and chemistry, which makes the prediction of actual nucleation rates a daunting task. Recently surfaces with well-characterized textures have been developed in order to control bubble nucleation (see below for examples). Surface textures can give rise to novel and complex phenomenology and are the ideal test case for nucleation theories. Before summarizing this phenomenology and describing the objectives of this focus article, let us give few examples of applications of such surfaces and explain why their function is connected to the nucleation of gas or vapor bubbles.

Surface textures enhance the hydrophobic/hydrophilic properties of a surface. A liquid on a textured surface can completely wet the surface corrugations (Wenzel state[5]) or remain suspended on top of the gas or vapor pockets entrapped in the corrugations (Cassie-Baxter state[6]). Due to the minimal liquid/solid contact, the Cassie-Baxter state is characterized by enhanced properties of the textured surface as compared to the corresponding flat one; the ensuing surface properties are known as *superhydrophobicity*. One of the first applications inspired by superhydrophobic surfaces is self-cleaning. In nature, plants and animals exploit the self-cleaning properties of superhydrophobic, textured, surfaces to keep their leaves and skin clean. This is the well-known case of the Lotus leaves, after which the self-cleaning effect is named: the Lotus effect.[7] Dirt cannot adhere strongly to the Lotus leaves and is picked up by (almost perfectly spherical) water droplets, which easily roll off of the leaves, thanks to the low *tilting angle*[8] of their textured superhydrophobic surface.

Under suitable conditions, the Cassie-Baxter state is metastable, which, on an proper timescale, evolves into the stable Wenzel state. This process can be used for the realization of implantable drug delivery systems:[9] the drug is embedded in a superhydrophobic mesh and is progressively released by contact with water when the transition to the Wenzel state advances. This system has been shown to be effective for more than two months in cancer treatment *in vitro*. A key aspect for this kind of applications is the design of materials with tailored and tunable wetting rates.

Another important application of bubble nucleation in medicine is for enhancing drug delivery. For instance, current anticancer therapeutics are unable to penetrate beyond blood vessels deep into cancerous tissues; this difficulty severely

[a]Electronic mail: simone.meloni@uniroma1.it
[b]Electronic mail: alberto.giacomello@uniroma1.it

limits the possibility of cancer treatment. However, it has been shown that remote mechanical activation of shelled microbubbles with ultrasound (cavitation) enhances drug delivery.[10] One limitation of this approach is the quick destruction of microbubbles, the agents inducing cavitation, at the relevant ultrasound amplitudes. In practice, microbubbles are stable for times (~30 s) which are too short as compared to the circulation of tumor drugs (~10 min). Another cavitation agent, nanocups, is capable of trapping and stabilizing gas bubbles against dissolution in the bloodstream; consequently nanocups can initiate and sustain cavitation for much longer times (approximately four times longer than microbubbles).[11] A critical feature of nanocups is that they must entrap a stable gas bubble in their cavities and be able to produce cavitation at ultrasound frequencies and intensities achievable with the existing diagnostic and therapeutic systems.

Another phenomenon associated to the (meta)stability and dynamics of the two phase liquid-gas system on complex surfaces is connected to underwater respiration of wetland insects, spiders, and plants.[12] Rough hydrophobic surfaces are capable of stabilizing the Cassie-Baxter state and thus realize an extended liquid-gas interface, which increases the oxygen uptake from the liquid. Thus the textured surface acts as a *physical gill*, allowing plants and animals to survive underwater. It has been speculated[13] that similar systems could provide enough oxygen for a human to survive underwater.

These few cases show the technological relevance of textured surfaces and their importance in controlling, enhancing, or preventing the formation of gas bubbles inside and outside surface corrugations, or the opposite process of wetting them (see Fig. 1).

Many aspects of equilibrium states of confined fluids are still unclear and even less is known about the kinetics and mechanism of transitions between the liquid and the vapor phases at complex surfaces. These latter aspects of the physics of confined fluids are the subject of the present focus article. An impressive amount of experimental, theoretical, and computational work has been accumulated in this field over the last couple of decades. Here we do not attempt to discuss the entire corpus of this research, for which the reader is encouraged to consult books[14] or more comprehensive reviews.[15] Rather, we take a relatively narrow path starting from the theories of vapor nucleation in the bulk and on simple (smooth or gently undulated) heterogeneous surfaces and arriving to modern concepts and ideas in the field of nucleation at textured surfaces. Along this path we will present and discuss a limited number of articles, which are neither necessarily the first article in each subject, nor the most cited. We selected those that, when put together like in a puzzle, give a comprehensive picture of the status of the field, of the (many) questions which remain to be addressed, and of the pitfalls of nucleation theories. We are aware that many more contributions would have deserved consideration and apologize in advance with their authors for the omission.

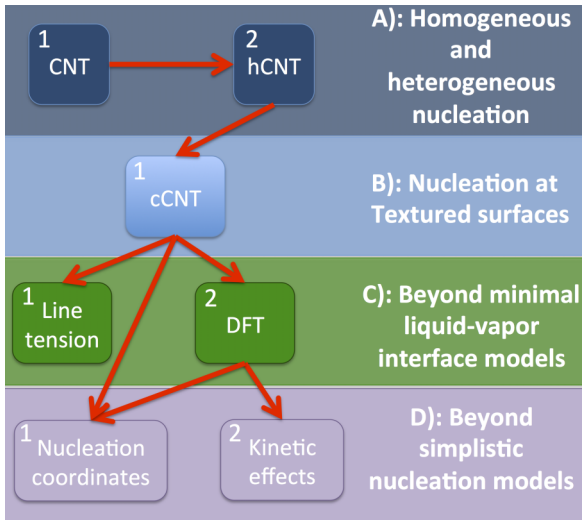

FIG. 2. Graphical representation of the sections of the article and their relation. The sections are divided into 4 groups. The first group contains the sections discussing the classical theory of homogeneous and heterogeneous nucleation. The second group contains (masinly) the continuum rare events method (CREaM), an extension of the classical nucleation theory to the case of confined fluids. The second group contains two sections extending the simple sharp interface model by (i) including the term relative to the three-phase contact line and (ii) a more realistic model of the interface among the three phases, and the effects of these models on the nucleation. Finally, the fourth group contains sections discussing more subtle effects on nucleation, in particular, (i) more advanced nucleation variables than the volume of vapor and (ii) kinetic effects going beyond the quasi-static nucleation hypothesis.

Figure 2 illustrates the structure of the article and the connections between the sections. We start from the well-established theories of bulk and heterogeneous nucleation on flat or gently undulated surfaces (panel (A)) and introduce their extensions to textured surfaces (panel (B)). Then, in the sections corresponding to panels (C) and (D), we discuss improvements over these classical descriptions, which can solve some of their limitations and improve their predictive power.

In Sec. II we discuss vapor nucleation in the bulk and describe it in terms of the classical nucleation theory (CNT); even this deceivingly simple case presents relevant theoretical challenges. In Sec. III we discuss the extension of CNT to simple heterogeneous cases: a flat or gently undulated solid surface. In Sec. IV we introduce some early and more recent

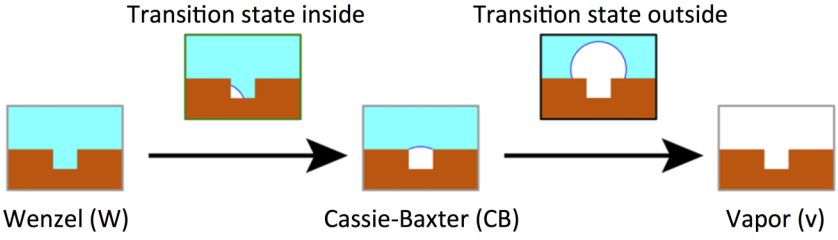

FIG. 1. Sketch of the nucleation of a vapor bubble inside and outside a pore. Adapted with permission from Giacomello *et al.*, Langmuir **29**, 14873 (2013). Copyright 2013 American Chemical Society.

macroscopic treatments of vapor nucleation at a textured surface. Secs. II-IV present theories that can be considered a classical description of vapor nucleation or of its opposite phenomenon, in which gas is replaced by liquid. They are based on the simple sharp interface model of the liquid-vapor system and on the assumption that the transition takes place *via* a quasi-static process in which the volume of the vapor bubble is the observable monitoring of the state of the system. In Secs. V–VIII we discuss theories, methods, and results that go beyond these assumptions. In Sec. V we consider the contribution of line tension to the free energy of a three-phase (solid-liquid-vapor) system, i.e., the term is associated to the length of the three-phase line. In Sec. VI we consider the effect of a finite-thickness, smooth interface between the phases. With some notable exceptions, most of the theories and models of nucleation pay little attention to the morphology of the vapor bubble along the process. This simplistic hypothesis is, probably, inspired by CNT, in which the bubble is spherical, and its volume is a good observable for describing the process. However, this assumption has no solid scientific ground when relatively complex confining environments are taken into account. In Sec. VII we discuss the effect of the choice of the order parameters, or nucleation variables, on the characterization of the nucleation process and its energetics. Even though it is not always made explicit, most classical models of nucleation and many microscopic simulations postulate that nucleation takes place in quasi-static conditions. This amounts to assuming that the system evolves so slowly that, for a given advancement of the process, it can always reach the configuration corresponding to the (local) minimum of the free energy. In Sec. VIII we discuss some of the artifacts associated with this assumption, and how it is possible to go beyond it. Finally, in Sec. IX we draw some conclusions and give a perspective on the present and future challenges in the field.

II. CLASSICAL NUCLEATION THEORY (CNT) FOR BULK SYSTEMS

At the beginning of each section, we indicate the panel of Fig. 2 to which it refers. The objective is helping the reader to understand what is the relation among the various sections and the specific position of each one in the taxonomy of the theoretical description of vapor nucleation. The present section is relative to panel (A.1) of Fig. 2.

CNT is the simplest and, perhaps, fundamental, theory of (bulk) nucleation. An exhaustive description and discussion of other, well-established bulk nucleation theories can be found, e.g., in the book by Kelton and Greer.[14] In CNT the system is assumed to be composed of two phases separated by a sharp (Gibbs) interface. The new phase is formed in the bulk of a pre-existing one occupying a given control volume, which is kept at a constant temperature and chemical potential. The probability density of observing a composite liquid-vapor system comprising, say, a vapor bubble of volume V_v, is proportional to the negative exponential of the relevant thermodynamic potential,

$$p(V_v) = \exp[-\beta \Delta\Omega(V_v)], \tag{1}$$

where $\Delta\Omega(V_v) = \Omega(V_v) - \Omega(0)$ is the grand potential of the composite system relative to the pre-existing phase and $\beta = 1/(k_B T)$ is the reciprocal of the temperature (in Boltzmann constant units). For the other ensembles, equations analogous to Eq. (1) hold; in the following the symbol Ω will be used in the general sense of thermodynamic potential of the given ensemble.

In the sharp interface model, the grand potential of a two-phase system reads

$$\Delta\Omega(V_v) = -\Delta P\, V_v + \gamma A, \tag{2}$$

where $\Delta P \equiv P_v - P_l$ is the difference between the pressure of the vapor and that of the liquid. γ is the surface energy relative to the interface and A the associated area; in the standard formulation γ it is taken to be the value of the flat liquid-vapor interface. Since $\gamma > 0$ the interface term always corresponds to an energetic penalty. Formulas analogous to Eq. (2) can be derived for other ensembles via Legendre transforms. For example, for the isothermal-isobaric ensemble, one gets

$$\begin{aligned}\Delta G(N_v) &= \Delta\Omega + P_v V_v + P_l V_l - P_l(V_v + V_l) \\ &\quad + \mu_v N_v + \mu_l N_l - \mu_l(N_v + N_l) \\ &= \Delta\mu\, N_v + \gamma A,\end{aligned}$$

where $\Delta\mu \equiv \mu_v - \mu_l$ is the difference between the chemical potential of the vapor and liquid phases, respectively, at the pressure of the barostat, and N_v is the number of particles in the vapor phase. In this ensemble one can relate the pressure difference with the undersaturation via $\Delta P \approx \rho_v(\mu_v(P_v) - \mu_v)$, where $\mu_v(P_v)$ is the chemical potential of the vapor at the pressure of the vapor bubble and ρ_v is the vapor bulk density (see Ref. 14 for more details). As we will see in the following, the formulation in terms of the grand potential is more convenient to derive theoretical descriptions of the liquid-to-vapor transition and to compare with the results of advanced simulation techniques, which typically compute the thermodynamic potential of an open control volume.

Assuming that the nucleation process is quasi-static, the liquid-vapor interface along nucleation is spherical because this shape minimizes the interfacial cost for any volume V_v. In other words, in CNT the nucleation path is a succession of spherical bubbles of growing radius. ΔP in Eq. (2) can be positive or negative depending on the thermodynamic conditions; this term represents the driving force for the phase transition.

For the case of a stable vapor phase nucleating within a metastable liquid, i.e., $\Delta P > 0$, $\Delta\Omega(V_v)$ has the shape shown in Fig. 3 characterized by a nucleation barrier $\Delta\Omega(V_v^*)$. The barrier is defined by the grand potential maximum occurring at a volume $V_v^* = (32\pi/3)\,(\gamma/|\Delta P|)^3$, which corresponds to the so-called critical nucleus of radius $R_c = 2\gamma/|\Delta P|$. For $V_v > V_v^*$ the free energy starts to decrease and the *thermodynamic force* favors the nucleus growth. The height of the barrier, $\Delta\Omega(V_v^*) = 16\pi(\gamma^3/\Delta P^2)$, determines how probable the transition from the initial metastable state to the final phase. The barrier depends on the thermodynamic conditions through ΔP and on the liquid characteristics through γ. When

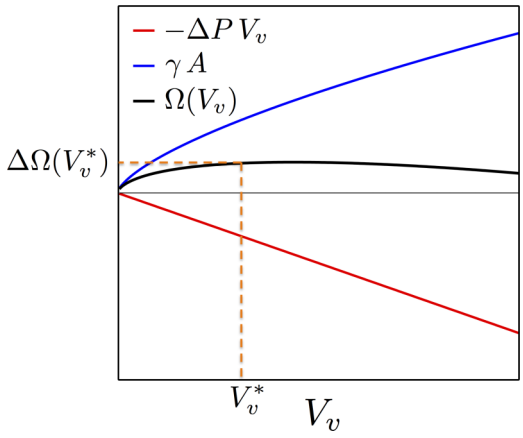

FIG. 3. Grand potential for the nucleation of a spherical vapor bubble in a bulk liquid, $\Omega(V_v)$ (black); the bulk $-(P_v - P_l)\, V_v \equiv -\Delta P\, V_v$ and interface γA contributions are represented in red and blue, respectively.

the barrier is much higher than the thermal energy of the system, $k_B T$, the transition is improbable, i.e., the initial metastable phase is long-lived.

Before exploring more complex cases, it is worth shortly analyzing some recent studies on the nucleation of vapor from its metastable liquid (*homogeneous nucleation*). Even for this allegedly simple case, for which CNT was initially formulated, many unclear aspects remain, as demonstrated by the conflicting results and conclusions of recent theoretical and computational works. Here we limit our attention mainly to two articles, Refs. 16 and 17, which discuss the limits of CNT. Homogeneous nucleation is also instrumental to introduce some of the modeling challenges of nucleation which are also valid for more complex, confined systems.

In Ref. 16, Shen and Debenedetti investigate the nucleation of vapor bubbles in a Lennard-Jones (LJ) liquid by umbrella sampling[18] (US). The number density of the system is used as the collective variable, i.e., the parameter monitoring the progress of nucleation. Indeed, in a liquid-vapor system, the total density in a control volume is a proxy for the volume of vapor in it. US is used to overcome the *rare event* problem, which is typical of processes characterized by a large free energy barrier such as the liquid-to-vapor nucleation. In these cases, the transitions from the metastable to the stable state are too infrequent to be simulated by *brute force* Monte Carlo (MC) or Molecular Dynamics (MD). At superheating $S_h \sim 8\%$, defined as $S_h \equiv (T_{\mathrm{sim}} - T_{\mathrm{sat}})/T_{\mathrm{sat}}$, where the subscripts indicate the simulated and saturation temperatures, respectively, a free energy barrier of $\sim 70\ k_B T$ was computed. The characteristic time for observing a nucleation event depends exponentially on the free energy barrier: $\tau \propto \exp[\Delta\Omega/k_B T]$. With a barrier of $\sim 70\ k_B T$, one could estimate $\gg 10^{30}$ molecular dynamics MD or MC (global) steps to observe a single nucleation event. This makes it clear why advanced sampling techniques are necessary to study gas and vapor nucleation. US consists in adding a pseudo-quadratic term $k/2(\theta(\mathbf{r}) - z)^2$ to the potential energy, where $\theta(\mathbf{r})$ is an observable that is able to characterize the nucleation process, the "collective variable," z is a realization (value) of this observable, and $\mathbf{r}$ is the $3N$ vector of the atomistic coordinates. The pseudo-quadratic term forces the system to visit and sample regions of the configuration space close to the condition $\theta(\mathbf{r}) = z$, including regions of low probability, e.g., the region of critical nucleus. In this way, US enhances the sampling, forcing the system to visit states that are not visited during the typical duration of a standard MD or MC. The effect of the biasing potential can be removed *a posteriori*, and one can compute the probability density function to observe a given value of the observable $\theta(\mathbf{r})$ in the equilibrium system, $p_\theta(z)$, and from this the Landau free energy,[19] $\Omega_\theta(z) = -k_B T \log p_\theta(z)$. From US simulations, one can also compute conditional averages or obtain qualitative information such as the most probable configurations of the system at a give value of $\theta(\mathbf{r})$. On the basis of US simulations, Shen and Debenedetti concluded that vapor bubbles with $R > R_c$ have a ramified shape, in contrast with the spherical shape of CNT.

Wang, Valeriani, and Frenkel[17] simulated an analogous system in thermodynamic conditions which are nominally[20] the same as those considered by Shen and Debenedetti. They used a different rare-event technique, the forward flux sampling (FFS).[21] In FFS a series of *milestones*, $\theta(\mathbf{r}) = \lambda_i$, are introduced which divide the configuration space into regions. The first milestone λ_A is chosen such that it is reachable by standard MD from the basin of the initial phase. This allows one to compute the flux Φ_A departing from the region A as the number of trajectories crossing the first milestone in a given time interval. The rate of the process Φ_B, which is the flux of trajectories coming from A and reaching the region of the final phase B, can then be expressed as the product of Φ_A with the probability to go from A to B without coming back to A, $p(\lambda_B|\lambda_A)$. In the presence of large free energy barriers, computing accurately $p(\lambda_B|\lambda_A)$ is very difficult if not impossible. However, $p(\lambda_B|\lambda_A)$ can be expressed as the product of the sequence of intermediate conditional probabilities $p(\lambda_{i+1}|\lambda_i)$, which are computed from the trajectories which reach the $(i+1)$th milestone coming from the i th, without returning to A. The distance between milestones should be chosen such that computing $p(\lambda_{i+1}|\lambda_i)$ with the desired accuracy is computationally feasible. This is the key ingredient of FFS for accelerating simulations of rare events. A significant difference between FFS and US, or other *conditional equilibrium* methods, is that FFS allows to reconstruct actual and complete nucleation trajectories. Moreover, FFS does not imply the hypothesis that the process is quasi-static.

Wang, Valeriani, and Frenkel performed FFS simulations using the volume of the largest bubble as the observable defining the milestones. This is a *local* observable to describe the nucleation as opposed to the global one used by Shen and Debenedetti. This observable is the atomistic analogue of the one used in CNT, V_v. The three key conclusions of Ref. 17 are (i) nucleation takes place *via* the formation of compact bubbles; (ii) despite the phenomenology is consistent with CNT, the FFS rate is much higher than that predicted by CNT; (iii) nucleation events are initiated by local hotspots, i.e., regions in which the kinetic energy of the particles is higher than the temperature of the system. The second

conclusion is somewhat mitigated by the authors' observation that CNT estimates are subject to considerable uncertainty. Indeed, given the exponential sensitivity of rates on free energy barriers, small statistical errors in the estimation of the value of surface tension have huge effects on the calculation of the nucleation rate.

The comparison between Refs. 16 and 17 underscores an important aspect in the modeling of nucleation at complex surfaces: the choice of the observable(s) describing nucleation has an influence on the nucleation barriers and rates (Sec. VII). As mentioned above, Wang, Valeriani, and Frenkel use the size of the largest vapor bubble, a *local* observable, while Shen and Debenedetti the (total) density of the sample, which is a *global* observable. In Ref. 17 it is remarked that a given value of the global observable can be realized with either a single large bubble or several smaller ones. Thus, the ramified structure observed by Shen and Debenedetti could be the result of this second process, which for entropic reasons might prevail in a quasi-static process/simulation (see Ref. 22). The fact that such a structure is not observed in FFS simulations may indicate that the ramified structure is not favored when kinetic effects are included. However, Meadley and Escobedo[23] have performed FFS simulations with both the global and the local order parameters and found no major differences in the nucleation mechanism between the two cases. Other possible explanations of the different shapes might be related to (i) slightly different thermodynamic conditions, with the closer to the spinodal conditions favoring ramified shape; and (ii) the finite size of the box together with periodic boundary conditions might affect the shape of the critical bubble.

Another key difference between Refs. 16 and 17 is the possible contribution of (local) fluctuations out of equilibrium, which are not present in US simulations and, in general, in all simulations which involve the sampling of conditional probabilities. The results of Ref. 17 suggest that nucleation can be triggered by local hotspots. This conclusion is, in turn, challenged by results of a recent brute force MD on very large samples.[24] In our opinion this question is not yet settled and deserves further investigation. In particular, the role of hotspots might be important in the case of heterogeneous nucleation, especially at textured surfaces, in which the presence of materials with different specific heats, conductivities, and/or the formation of an insulating layer of vapor might increase the time the system takes to relax local fluctuations to equilibrium.

Other approaches going beyond the capillarity approximations are available in the literature,[14] which for reasons of brevity are not discussed here. In particular, the kinetic theory of nucleation developed by Ruckenstein and coworkers[25,26] relaxes the hypothesis of constant surface tension by computing the emission and absorption rates of particles of the new phase from/to the nucleus via a kinetic equation. This theory, originally developed for homogeneous vapor-to-liquid and liquid-to-solid nucleation, has also been extended to the homogeneous liquid-to-vapor case.[27]

III. HETEROGENEOUS CLASSICAL NUCLEATION THEORY (HCNT)

This section is relative to panel (A.2) of Fig. 2.

CNT can be generalized to heterogeneous systems, i.e., extended surfaces. It turns out that in such conditions nucleation is greatly enhanced, such that in practical systems nucleation is always heterogeneous. Here we consider two classical cases:[4] nucleation at smooth (flat) surfaces and nucleation at surfaces with gentle undulations. Along the description of these two cases, we will introduce some of the fundamental ingredients of vapor nucleation at textured surfaces.

Under the same assumptions of homogeneous CNT (sharp interface model, quasi-equilibrium process), in these simple heterogeneous cases, it can be shown that the vapor nucleus is a spherical cap. This cap forms with the surface a contact angle $\cos\theta = \cos\theta_Y \equiv (\gamma_{vs} - \gamma_{ls})/\gamma_{lv}$, where θ_Y is the Young contact angle and γ_{vs}, γ_{ls}, and γ_{lv} are the surface tensions of the vapor-solid, liquid-solid, and liquid-vapor interfaces, respectively (see Fig. 4(a)). For a given value of the vapor bubble radius, the condition on the contact angle determines the volume V_v of the bubble and the value of the three vapor-solid, liquid-solid, and liquid-vapor areas, A_{vs}, A_{ls}, and

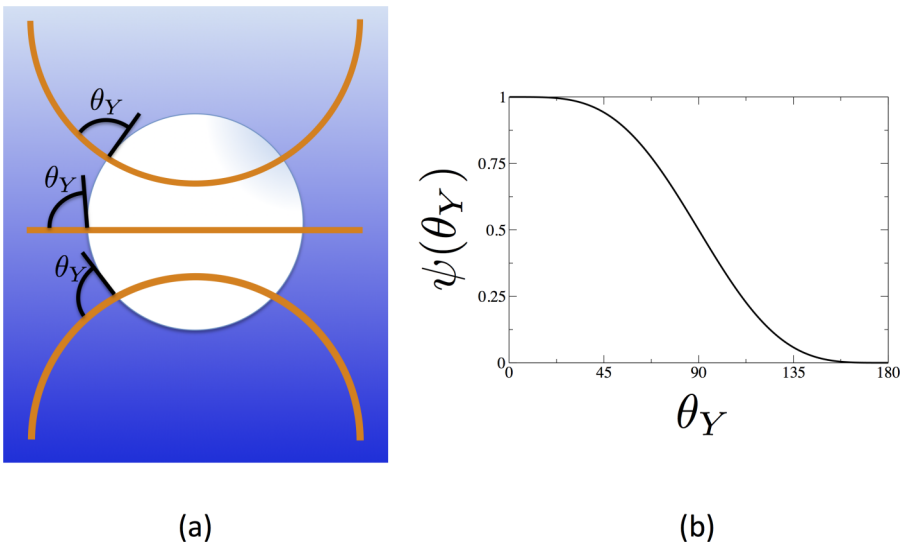

FIG. 4. (a) Configuration of a critical vapor bubble on a concave (top), flat (middle), and convex (bottom) surface of contact angle θ_Y. The solid domain, not shown, is in the lower part of the figure for all the three substrates. This scheme is based on the classical book by Skripov.[4] (b) Wetting angle function (see Eq. (3)).

A_{lv}. Under the same assumptions of CNT, and given the conditions listed above, the grand potential $\Delta\Omega(V_v)$ reads[4]

$$\begin{aligned}\Delta\Omega(V_v) \equiv \Omega(V_v) - \Omega(0) &= -\Delta P\ V_v + (\gamma_{vs} - \gamma_{ls})A_{vs} + \gamma_{lv}A_{lv} \\ &= -\Delta P\ V_{sp}\left[\frac{1}{4}(1+\cos\theta_Y)^2(2-\cos\theta_Y)\right] \\ &\quad + \gamma A_{sp}\left[\frac{1}{4}(1+\cos\theta_Y)^2(2-\cos\theta_Y)\right] \\ &= \Delta\Omega_{CNT}(V_{sp})\left[\frac{1}{4}(1+\cos\theta_Y)^2(2-\cos\theta_Y)\right], \qquad (3)\end{aligned}$$

where V_{sp} and A_{sp} are the volume and area of the sphere having the same radius as the cap, respectively. The reference grand potential $\Omega(0)$ is taken to be the one corresponding to the liquid wetting the surface; $\Delta\Omega_{CNT}(V_{sp})$ is the grand potential of the homogeneous case defined in Eq. (2). The term $\psi(\theta_Y) = \left[\frac{1}{4}(1+\cos\theta_Y)^2(2-\cos\theta_Y)\right]$, which depends only on the contact angle, is usually called *wetting angle function* and has the monotonically decreasing trend shown in Fig. 4(b).

Since the dependence of Eq. (3) on V_{sp} is only through $\Delta\Omega_{CNT}(V_{sp})$, it follows that the radius of the critical nucleus is the same for the homogeneous and heterogeneous cases; the critical volume, instead, since it is referred to a spherical cap, is always smaller in the heterogeneous case (Fig. 4(a)). Since $\psi(\theta_Y) < 1$, the barriers for the two cases can be quite different already at small values of θ_Y. For neutral surfaces, i.e., $\theta_Y = 90°$, the heterogeneous barrier is half the homogeneous one. Moving in the hydrophobic domain ($\theta_Y > 90°$), the barrier is further reduced, and for surfaces with a contact angle of ~130°, which can be achieved with well-established fabrication approaches, the nucleation barrier is only 10% of the homogeneous one.

A further extension of the classical nucleation theory is its application to gently undulated surfaces. With "gently undulated" we refer to surfaces on which the nucleation path is not significantly changed with respect to the perfectly flat surface case. This definition is somewhat vague as one should first prove under which conditions the undulations do not affect the path; a more formal approach to the problem is discussed in Sec. IV. For the time being, we use the heuristic definition given above. A qualitative argument[4] to understand the effect of undulations, based on a parallel with the case of planar surfaces, is given in Fig. 4(a). For a vapor bubble of given radius, a convex undulation, which protrudes in the fluid region, results in a higher surface/volume ratio with respect to the case of a flat surface, which, in turn, has a higher surface/volume ratio with respect to the case of a concave surface. Since the surface term is the penalty term, and the volume term is the driving force of the phase transition, the energy barrier follows the same order of the surface volume ratio.

As mentioned above, the analysis of gently undulated surfaces is valid as long as the nucleation path does not deviate from the simple one illustrated in Fig. 4(a). One possible alteration of the nucleation path is the presence of intermediate metastable states between the liquid and vapor states: an example is the Cassie-Baxter state discussed in the Introduction, in which gas/vapor pockets are found within surface corrugations. In this case one must first consider the process of nucleation of a gas/vapor bubble within the surface textures, bringing the system from the completely wet Wenzel state to the Cassie-Baxter one. The Wenzel to Cassie-Baxter transition can be seen as a gas/vapor nucleation process. Indeed, recent atomistic simulations (e.g., Refs. 28–31) have shown that, in the absence of dissolved gasses, the Wenzel to Cassie-Baxter transition proceeds *via* the formation of a (rather complex) vapor bubble inside surfaces cavities. As we discuss in detail in Sec. IV, the Wenzel to Cassie-Baxter transition can be described in macroscopic terms starting from the heterogeneous CNT formulated in Eq. (3).

The more general case of miscible and partly miscible gasses introduces additional complications to the theoretical description of the nucleation process. To the best of our knowledge, its discussion from *first principles* is presently limited to the cases of infinitely fast or infinitely slow transitions. In such limits the problem reduces to the completely immiscible and to the vapor case, respectively.

Considering the observations above, in the following we will focus on vapor nucleation in textured surfaces, discussing also results concerning the Wenzel to Cassie-Baxter transition and the reverse one, Cassie-Baxter to Wenzel.

IV. MACROSCOPIC MODELS OF NUCLEATION AND CLASSICAL NUCLEATION THEORY IN CONFINED ENVIRONMENTS (CCNT)

This section is relative to panel (B.1) of Fig. 2.

Perhaps the earliest theory of the Wenzel to Cassie-Baxter transition is the one due to Patankar.[32] Actually, the author focused on the opposite process, i.e., the wetting of surface textures by a macroscopic droplet deposited on top of them in the Cassie-Baxter state. Since the curvature of the droplet is much larger than the space between surface corrugations, Patankar assumed that $\Delta P \approx 0$ and only surface terms matter (cf. the first equality in Eq. (3)). The liquid-vapor meniscus is assumed to remain flat and its shape not to change during the wetting/evaporation process (see Fig. 5). This hypothesized mechanism leads to a free energy profile which is linear in the volume V_v, with a discontinuity at the beginning of

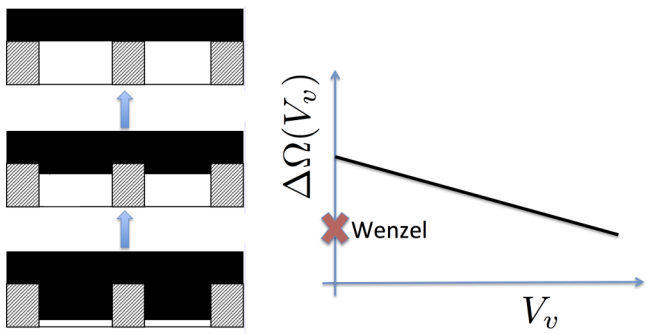

FIG. 5. Sketch of the Patankar-like vapor nucleation model: the liquid detaches from the bottom of the surface texture forming a flat bubble. This path is obtained reversing the wetting path originally proposed by Patankar. Adapted with permission from N. A. Patankar, Langmuir **20**, 7097 (2004). Copyright 2004 American Chemical Society.

the nucleation process, when the liquid detaches from the bottom wall and the liquid-solid interface is replaced by two parallel interfaces (liquid-vapor and solid-vapor). As soon as this first vapor layer is formed, if the chemistry of the surface is hydrophobic, the free energy decreases until the Cassie-Baxter minimum is reached. The discontinuity mentioned above disappears if one introduces finite temperature effects (capillary waves[33]) or, which is somewhat related, if the liquid-vapor interface is diffuse (see Sec. VI).

The mechanism shown in Fig. 5 is assumed *a priori*, while one may desire a predictive theory valid for generic geometries. Thus, additional effort has been spent along the years to go beyond this mechanism; despite the significant improvements, these attempts are still based on *a priori* hypotheses on the wetting/nucleation mechanism.[34,35] Another continuum theory — the continuum rare events method (CREaM) — has been recently proposed[29] to study the nucleation of vapor in surface textures or the reverse process of wetting from the Cassie-Baxter state. This is, in spirit, an extension of CNT to the case of textured surfaces, where additional metastable states and nucleation paths are accounted for. CREaM consists in a conditional minimization of the grand potential in Eq. (3) and, consistently with CNT, it is based on the assumption that nucleation is a quasi-static process. Thus, for each value of the bubble volume V_v, the system, which is defined by the liquid-vapor (Σ_{lv}), solid-liquid (Σ_{sl}), and solid-vapor (Σ_{sv}) interfaces, relaxes to the conditional minimum of the grand potential. The minimization conditioned to $V_v = const$ brings to the following two conditions on Σ_{lv}: the first is the usual Young equation for the contact angle,

$$\cos\theta_Y = \frac{\gamma_{sv} - \gamma_{sl}}{\gamma_{lv}}. \tag{4}$$

Here the contact angle is measured with respect to the local tangent to the actual solid surface, and *not* with respect to nominal surface of the solid. The second condition on Σ_{lv} is the modified Laplace equation,

$$J = \frac{P_l - P_v - \lambda}{\gamma_{lv}}, \tag{5}$$

where $J \equiv 1/R_1 + 1/R_2$ is twice the mean curvature of the liquid-vapor interface and λ the Lagrange multiplier necessary to impose the volume constraint at the (unconditional) extrema of the grand potential $\lambda = 0$ and the usual Laplace equation is recovered. In practice, conditions (4) and (5) prescribe that the nucleation path is composed by a sequence of menisci having *constant curvature* and meeting the solid surface with the Young contact angle. In the following we will take this CNT for confined geometries, cCNT, as reference for more advanced treatments of nucleation at complicated solid surfaces.

For simple surface textures, e.g., a 2D rectangular groove, it is possible to identify all the liquid-vapor interfaces satisfying Eqs. (4) and (5). At variance with bulk and heterogeneous nucleation at smooth surfaces, in textured surfaces there can be several distinct local conditional minima of the grand potential, each corresponding to one $\Sigma_{lv}(V_v)$. Therefore, the nucleation path might consist of several branches with different morphologies. A (natural) criterion to choose the nucleation path among the many possible branches is that of minimum free energy: for each V_v, one selects the surface $\Sigma_{lv}(V_v)$ corresponding to the absolute conditional minimum of the grand potential; then, from the sequence of conditional minima, the nucleation path can be constructed. The above criterion renders the most probable configuration in the quasi-static hypothesis but has some limitations. For example, at the conjunction of two different morphologies, the meniscus jumps from one configuration to the other, and this might result in discontinuities in the profile of free energy or its derivative(s). Other limitations will be shown below.

For the 2D rectangular groove, the nucleation path is shown in Fig. 6, together with the corresponding grand

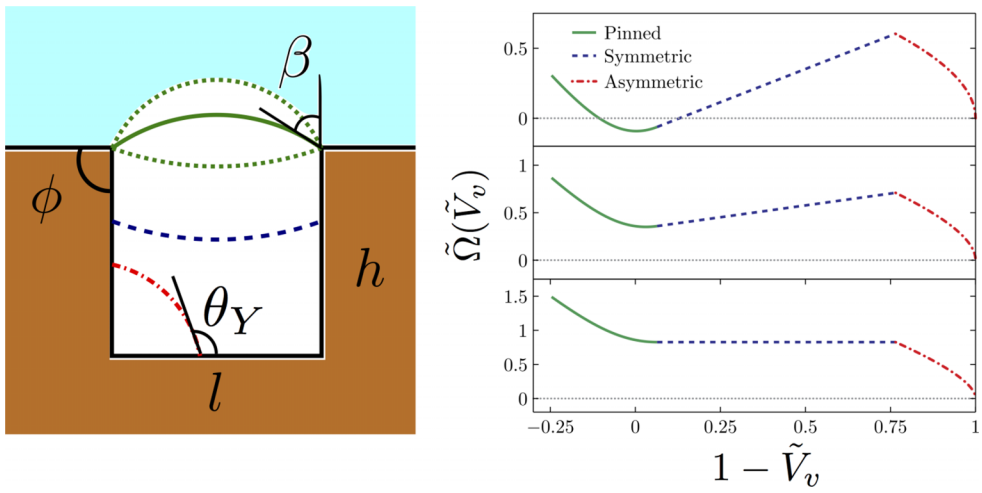

FIG. 6. Liquid meniscus corresponding to the various branches of the CREaM vapor nucleation path in a square 2D pore and the corresponding (nondimensional) grand potential profile. The red portion of the path corresponds to the formation of a vapor bubble in one of the bottom corners of the pore. The blue portion corresponds to the ascending symmetric meniscus, after the morphological transition from the bubble-in-the-corner configuration. Green corresponds to the pinning of the meniscus at the upper corners of the pore. Adapted with permission from Giacomello *et al.*, Phys. Rev. Lett. **109**, 226102 (2012). Copyright 2012 American Physical Society.

potential profile. The cCNT path and the related grand potential are in fair agreement with rare event atomistic simulation results.[29] For a rectangular groove, cCNT predicts a nucleation path for the formation of a vapor layer in the texture consisting of three branches. The process starts with the formation of a bubble in a corner of the pore (Fig. 6, dotted-dashed red curve), which then transforms into a symmetric meniscus spanning the entire pore (dashed blue curve) until it gets pinned at the corners of the pore (green). In the first branch of the path, the liquid-vapor interface breaks the symmetry of the system. Other paths exist satisfying the symmetry of the system, which however have associated higher barriers. Such a behavior, with both symmetric and asymmetric nucleation paths, was observed in recent experiments.[36]

It is worth remarking that the assumptions on which any CNT theory, bulk, heterogeneous, and confined, is based on (quasi-static process, sharp interface model, volume of the vapor bubble as the order parameter) are rather general and are valid for other nucleation processes as well. Thus, for example, cCNT results are in agreement with crystal nucleation in a pore studied via a 2D Ising model.[37] An important consequence of these hypotheses is that the nucleation path identified by homogeneous, heterogeneous, and confined CNT *does not depend on the pressure of the system* ΔP. Indeed, since the minimization of the grand potential is made at fixed V_v, the related pressure term in the free energy (Eq. (3)) is identical for all possible conditional minima and thus plays no effect on their relative grand potential value.

cCNT allows us to predict the nucleation path at (plane and) textured surfaces, i.e., the most likely path bringing the surface from the complete wet state, Wenzel, to the complete vapor state. In Ref. 38 it has been shown that this path can be non-trivial, possibly consisting of the union of several branches with different morphologies of the meniscus and characterized by the presence of an intermediate partially wet (Cassie-Baxter) state whose existence depends on the thermodynamic conditions and on the surface topography. Several regimes have been identified depending on the *nucleation number* $N_{nu} \equiv L\gamma_{lv}/|\Delta P|$, where L is a characteristic length of the surface texture which is introduced to obtain a dimensionless number. In order to show this, Eq. (5) is cast into a more convenient dimensionless form,

$$\tilde{\lambda} = -(\tilde{j} + N_{nu}), \tag{6}$$

with $\tilde{j} = J\,L$ and $\tilde{\lambda} = \lambda\,L/\gamma_{lv}$. In this form, the modified Laplace equation suggests that the sign of the *thermodynamic force* $\tilde{\lambda}$ — and thus the existence and position of the free energy maxima — depends on the value of N_{nu} which, in turn, depends on the ratio of the bulk driving force ΔP to the interface resistance γ_{lv}. Figure 7 shows how N_{nu} affects the nucleation mechanism; this dependence is studied via a graphical method based on Eq. (6).[38] First, the nucleation path, which

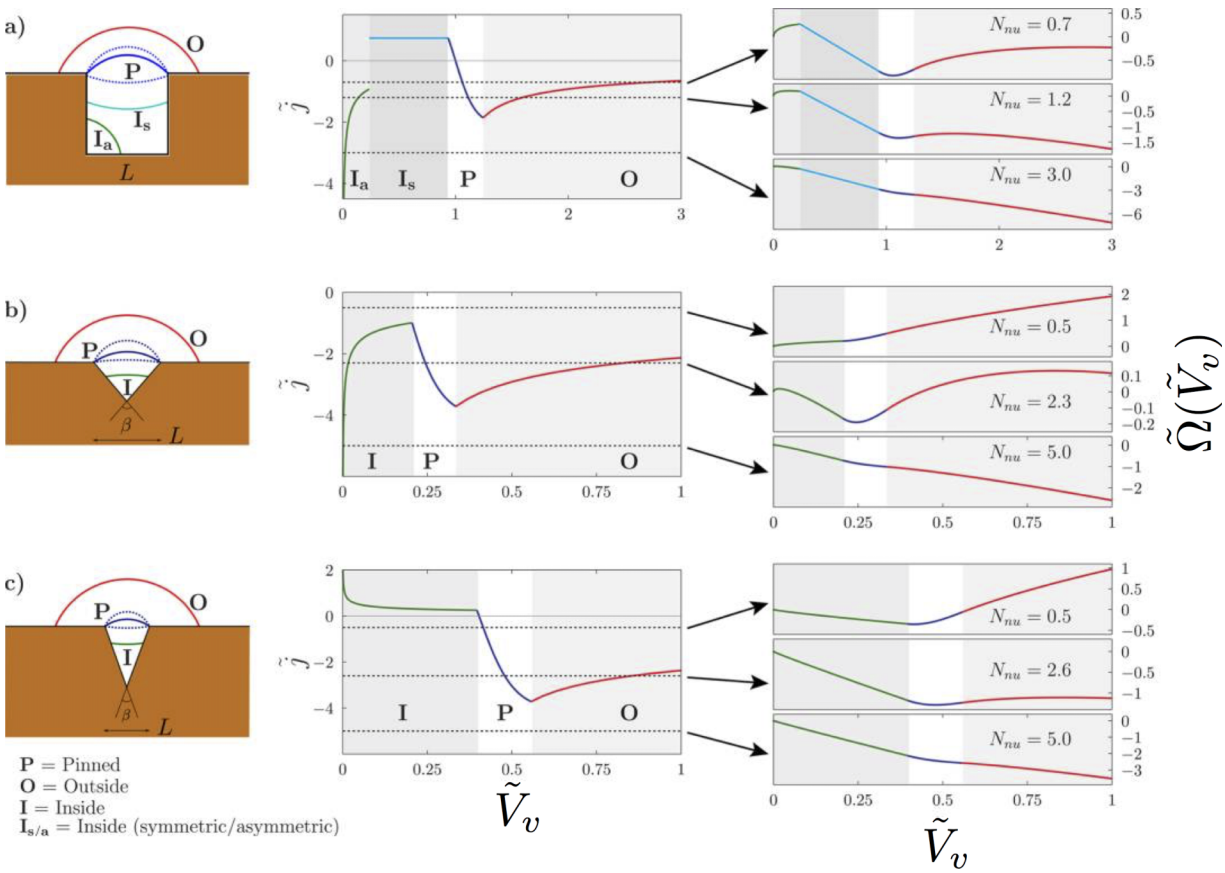

FIG. 7. (Left) Nucleation paths for (a) a 2D squared pore and 3D (b) wide and (c) narrow conical crevice. (Center) Nondimensional curvature corresponding to the nucleation paths reported in the left panel. Dashed lines represent nucleation number, N_{nu}. (Right) Grand canonical potential corresponding to the various values of N_{nu} reported in the central panel. Adapted with permission from Giacomello *et al.*, Langmuir **29**, 14873 (2013). Copyright 2013 American Chemical Society.

according to cCNT is unique for all pressures, is identified by conditional minimization; this can be done analytically for simple geometries[38] or with the aid of numerical tools, such as the Surface Evolver,[39] for more complicated textures;[40] the nucleation path allows one to compute the dimensionless curvature $\tilde{j}(\tilde{V}_v)$ along the process (second column of Fig. 7). Second, by plotting on the same graph $\tilde{j}(\tilde{V}_v)$ and $-N_{nu}$, one readily identifies maxima and minima of the grand potential along the nucleation path, which can occur either when $\tilde{\lambda} = 0$ ($\tilde{j} = -N_{nu}$ as per Eq. (6)) or at morphological transitions of the liquid-vapor interface. Finally, integrating $\tilde{\lambda}$ one obtains the grand potential profiles at the given value of $-N_{nu}$ (third column of Fig. 7). Depending on the value of N_{nu}, one can identify three nucleation regimes characterized either by the number or position of the barriers. For instance, in the case of the square pore, the $N_{nu} = 0.7$ case corresponds to a two-step process with the inner barrier occurring at the morphological transition between the bubble in a corner and the flat meniscus; at $N_{nu} = 1.2$, the process is still a two-steps one but the inner barrier is within the domain. Finally, for $N_{nu} = 3.0$ the bubble-in-the-corner nucleation is a single step process with only the inner barrier in the bubble-in-the-corner domain.

Figure 6 shows that the nucleation path identified by extending the CNT framework to textured surfaces has a discontinuity in correspondence of the point in which the liquid-vapor surface of minimum energy changes morphology along nucleation. This discontinuity is unphysical because the nucleation process must take place along a continuum macro- or microscopic dynamics. This puzzling result can be ascribed to the assumption of all versions of CNT that the conditional minimization should be done with respect to V_v; while this assumption is justified for most of the nucleation path, along which it follows the "valleys" of the grand potential landscape, it fails where the path switches from one valley to another.[30] A similar problem is present also with other well-established atomistic simulation techniques based on conditional sampling (see Sec. VII).

Another problem common to all the CNT frameworks, homogeneous, heterogeneous, and confined, is that they cannot predict the liquid and vapor spinodals,[41] i.e., the conditions for which the barrier for the liquid-vapor transition goes to zero.

In Secs. V–VIII, we will introduce and discuss theories, methods, and results going beyond the CNT assumptions. First, we consider possible additional terms to the grand potential of Eq. (3), in particular the line tension. Second, we consider the effect of diffuse interfaces which, for example, capture the spinodals as opposed to the sharp interface model. We then discuss observables other than V_v that can be used to monitor the nucleation process. Finally, we discuss kinetic effects which relax the quasi-static assumption.

V. LINE TENSION

This section is relative to panel (C.1) of Fig. 2.

In the fluid model adopted in Secs. II–IV (Eq. (3)), we considered bulk and surface contributions. However, in nanoscale systems the contribution of line tension to the grand potential might become relevant and thus influence nucleation.[42,43] This term is the energy gain or penalty proportional to the length of the three-phase contact line l_{slv} (the line determined by the intersection between the liquid-vapor interface and the solid surface). With this additional term, the grand potential reads

$$\Delta\Omega(V_v) = -\Delta P\ V_v + (\gamma_{vs} - \gamma_{ls})A_{vs} + \gamma_{lv}A_{lv} + \tau\, l_{slv}, \qquad (7)$$

where τ is the line tension. The effect of line tension on equilibrium and kinetic properties of multiphase systems is much debated in the literature. Values ranging from 10^{-6} to 10^{-11} N, with positive and negative signs, have been reported. This large uncertainty on the magnitude and sign of the line tension makes it difficult to assess the relevance of this term and the length scales where it plays a role. In addition, the definition of line tension is intrinsically troublesome because terms not directly related to it also scale with l_{slv}.[44,45]

Sharma and Debenedetti[46] investigated this issue for the case of capillary evaporation; in particular, they studied nucleation of vapor between two hydrophobic plates by atomistic simulations using FFS. They found that the barrier scales linearly with the distance between the plates in the range $d = 9$–14 Å. Using an approximate nucleation path and typical values for the surface and line tension, $\gamma = 0.07$ N/m and $\tau = 10^{-10}$ N, respectively, they estimated that the line contribution controls the height of the free energy barrier.

It is interesting to compare this result with the recent experimental work of Guillemot *et al.*,[47] who have shown that including the line tension term leads to heterogeneous CNT predictions consistent with the experimental results. The value of the line tension which must be used in the heterogeneous CNT model in order to match the experimental data is $\tau \approx -3 \times 10^{-11}$ N, which has a different sign than in the atomistic results of Ref. 46.

The two references discussed above[46,47] well illustrate the interest in accounting for nanoscale effects in heterogeneous nucleation. However, the value of line tension depends (i) on the definition adopted[44] and (ii) on the macroscopic nucleation path which is assumed in order to match the experimental or atomistic computational data (typically nucleation rates). Preliminary results suggest that an accurate modeling of the nucleation path, obtained without assuming any *aprioristic* hypothesis on the mechanism, can explain some nanoscale observations without invoking line tension.[48] In a sense, line tension is often used as an effective notion, encompassing many nanoscale effects with different origins; this results in a broad scattering of line tension values and prevents Eq. (7) from being predictive in generic cases. Overall the relevance of the line tension in nanoscale heterogeneous nucleation can still be considered an open question deserving additional experimental, theoretical, and computational investigations.

VI. DIFFUSE INTERFACE MODELS: DENSITY FUNCTIONAL THEORY (DFT)

This section is relative to panel (C.2) of Fig. 2.

One of the assumptions at the basis of CNT and its extensions is the sharp interface model of the multiphase

system. A further hypothesis which is implied in this "capillarity approximation" is that the value of surface tension(s) is constant and equal to the value of a flat interface. As we mentioned above, one of the consequences of these assumptions is that the barrier for the phase transition is never zero, for whatever degree of superheating/supersaturation (see Fig. 3). This is against the experimental evidence of spinodal transitions, i.e., barrierless transitions from the original to the new phase.[41] In addition, the hypothesis that the interface between two phases is sharp conflicts with the atomistic (or molecular) nature of fluids. Such effects might become relevant in nanoscale confinement or for extremely small critical nuclei, like close to spinodal conditions, see, e.g., Ref. 49 dealing with homogeneous drop nucleation. In order to illustrate these features, in the following we compare sharp and diffuse interface results for two paradigmatic cases, nucleation in a slit pore and in a 3D square cavity.

Several authors have investigated the effects of a diffuse interface on heterogeneous nucleation. Talanquer and Oxtoby[50] have considered the case of bulk and heterogeneous nucleation of a liquid droplet and the opposite phenomenon of nucleation of a vapor bubble in a slit pore. The authors extensively discuss their results for the nucleation of a confined liquid droplet but mention that analogous results have been obtained for the nucleation of a vapor bubble: "The behavior of critical bubbles under partial wetting (partial drying) conditions qualitatively resembles that of critical droplets under partial drying (partial wetting) conditions." This is not surprising and can be understood considering the sharp interface model, noticing that this model does not depend on the nature of the initial and final phase. Having these remarks in mind, following the original article we report results for the nucleation of a liquid droplet.

Reference 50 compares the results of the so-called gradient approximation to the (classical) density functional theory (DFT) and the sharp interface model. As the name suggests, DFT assumes that the grand potential of the system is a functional of the fluid density, approximately expressed as

$$\Omega[\rho(\mathbf{x})] = \int d\mathbf{x}\, [f[\rho(\mathbf{x})] - \mu\rho(\mathbf{x})] + \frac{K}{2}\int d\mathbf{x}\, |\nabla\rho(\mathbf{x})|^2 + \int d\mathbf{x}\, \Phi(\mathbf{x})\rho(\mathbf{x}), \quad (8)$$

where $f[\rho(\mathbf{x})]$ is the local Helmholtz free energy density, the square gradient term acts as a *penalty* associated with the liquid-vapor interface, and $\Phi(\mathbf{x})$ takes into account the interaction between the fluid and the solid walls, determining its solvophilicity/phobicity. The density $\rho(\mathbf{x})$ minimizing the grand potential Eq. (8) is the equilibrium density. DFT allows one to determine the properties of the stable and metastable states of a system, namely, the liquid and vapor phase between the walls of the slit pore in the present case.

DFT calculations also allow one to compute the binodal curve, i.e., the line where the (confined) liquid and vapor phases coexist, and how it depends on the distance between the walls. Figure 8(a) shows the binodal curve in the $\Delta\tilde{P} \equiv \tilde{P}_v - \tilde{P}_l$ *vs* $1/\tilde{L}$ plane, with $\Delta\tilde{P}$ and $\tilde{L}$ the nondimensional pressure difference and distance between the walls. For reference, the binodal curve obtained from the sharp interface model is also reported. A first important qualitative difference between the two curves is that in the DFT case, the binodal curve ends at a critical value of L. Below that value, which is determined by the thickness of the interface, a single state remains. In general, it is seen that the sharp interface model is able to describe the equilibrium properties of the system at large wall separations, while it becomes less accurate with increasing confinement $1/L$. In addition, DFT gives access to the spinodal lines, i.e., the loci of the $\Delta\tilde{P}$ *vs* $1/\tilde{L}$ plane where the metastable phases become unstable.

DFT can also be used to compute the properties of critical nuclei.[51,74] Consistently with the sharp interface model, DFT, in the functional form used by Talanquer and Oxtoby, predicts two morphologies of the critical nucleus for the case of the slit pore. The first corresponds to a drop at one wall (or, for liquid-to-vapor nucleation, to the equivalent vapor bubble). The second consists in a tube spanning the slit pore (or the

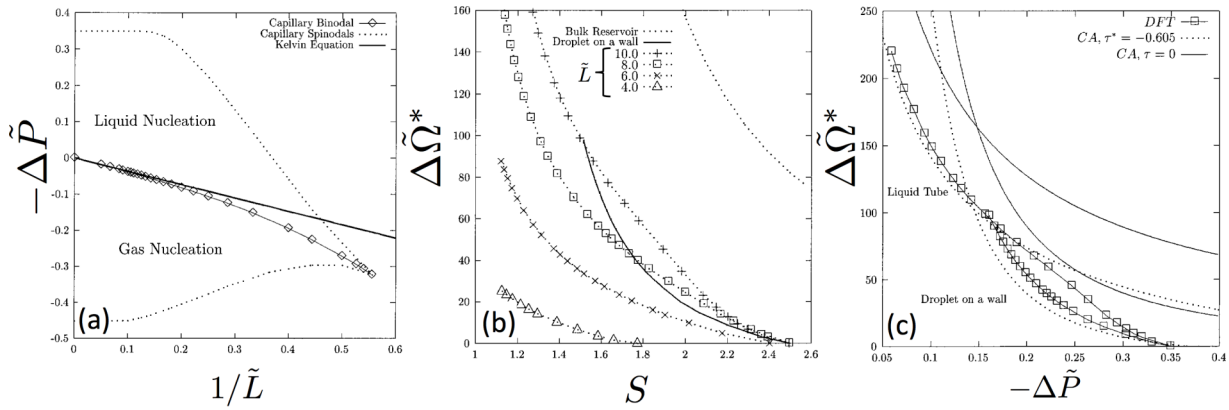

FIG. 8. (a) Binodal (solid lines) and spinodal (dotted line) curves for a van der Waals liquid confined within a slit pore as computed by DFT. For reference, the Kelvin equation, i.e., the binodal curve predicted by the sharp interface model, is also reported (thick solid line). (b) Free energy barriers for the tube and bubble nucleation paths as a function of supersaturation $S \equiv -\Delta P/P_{sat}$. For the tube mechanism, the barrier is reported for several values of the nondimensional distance between the walls, $\tilde{L}$. (c) Barriers for the tube and bubble nucleation paths as a function of the nondimensional difference of pressure for the DFT (squares) and sharp interface models (solid lines: without line tension; dashed lines: with line tension). Reproduced with permission from J. Chem. Phys. **114**, 2793 (2001). Copyright 2001 AIP Publishing LLC.

equivalent vapor cavity), and the value of the corresponding barrier depends on the distance between the walls, increasing with L. In addition, as for the homogeneous case, the barrier depends on the saturation $S = \equiv -|\Delta P|/P_{sat}$ (Fig. 8(b)). The main difference between DFT and cCNT results is quantitative, with the latter theory significantly overestimating the barrier when the spinodal is approached (Fig. 8(c)). This behavior is due to the fact that the critical nucleus shrinks in moving towards the spinodal conditions becoming of size comparable to the thickness of the diffuse interface, a phenomenon that cannot be captured in the capillarity approximation.

DFT has also been also used to study vapor-to-liquid nucleation in textured surfaces containing 3D square pores.[52] We rely on the qualitative symmetry between liquid-to-vapor and vapor-to-liquid nucleations to discuss the effect of the diffuse interface on bubble nucleation. Generally speaking, three states exist: a system containing only vapor (which for liquid-to-vapor nucleation would correspond to the Wenzel state), liquid filling the pore with vapor outside (denominated *pore-filled* and corresponding to Cassie-Baxter), and only liquid (corresponding to vapor). Depending on the thermodynamic conditions and on the geometry and chemistry of the surface, not all these states are (meta)stable and different nucleation mechanisms may be identified. Liu *et al.* have computed a "phase diagram" of nucleation mechanisms for a pore with a *mouth* of prescribed dimension as a function of the chemical potential μ and of the fluid/solid interaction strength, which can be related to the contact angle (Fig. 9). The graph contains six domains corresponding to six different mechanisms. Some of these mechanisms consist in a single step, when either the vapor or the pore-filled state is not stable. Other mechanisms involve two steps, when the vapor and pore-filled states are both metastable; in these cases the thermodynamic conditions determine which of the vapor–pore-filled or pore-filled–liquid has associated the higher barrier. Finally, at high chemical potential and fluid-solid interaction strength vapor and pore-filled states are both unstable, and the system is in the so-called textured surface spinodal domain (regions I), in which a system prepared in the vapor state undergoes a barrierless transition to the liquid state.

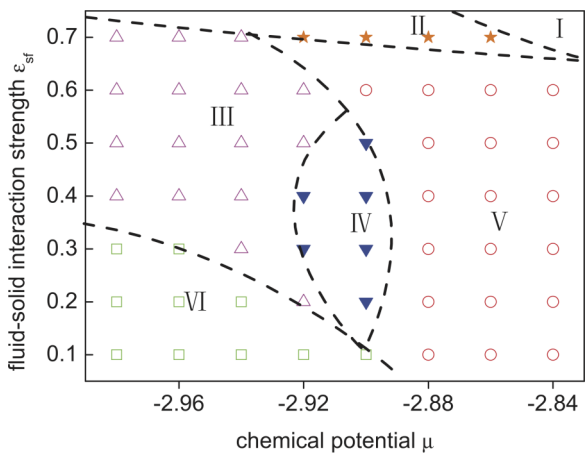

FIG. 9. Phase diagram of vapor-to-liquid nucleation mechanisms for a van der Waals fluid as obtained from NEB-DFT calculations. The nucleation mechanisms corresponding to the six regions are (I) the spinodal condensation, (II) single barrier with critical nucleus outside the pore, (III) double barriers with the highest one corresponding to the critical nucleus outside the pore, (IV) double barrier with the highest one corresponding to the critical nucleus inside the pore, (V) single barrier with critical nucleus inside the pore, and (VI) homogeneous nucleation. Reproduced with permission from J. Chem. Phys. **137**, 104701 (2012). Copyright 2012 AIP Publishing LLC.

By comparing the diffuse interface results[52] in Fig. 9 with analogous sharp interface model calculations[38] (also discussed in Sec. IV), it is clear that most of the complex nucleation phenomena are captured by the simpler model and determined by the value of the nucleation number N_{Nu}. Indeed, the latter approach still predicts the correct trend for the internal and external barriers with the chemical potential and with solvophilicity/phobicity. On the other hand, strictly speaking, the barriers never go to zero. However, for any practical purpose, one could imagine that when the barrier is of the order of few k_BT, the system undergoes a spinodal transition and the sharp interface model could still be used to reproduce the phase diagram of Fig. 9. However, since the sharp interface and DFT barriers may differ significantly when the system approaches the spinodal, we expect the sharp interface model predictions for regions I and II to be less accurate.

VII. COLLECTIVE VARIABLES FOR THE NUCLEATION PATH

This section is relative to panel (D.1) of Fig. 2.

The mechanism and energetics of vapor nucleation at complex textured surfaces has been investigated also by atomistic simulations. This approach avoids to resort to any *a priori* assumptions on the density field, which is implicit in the continuum models discussed above. Apart for the case of nanoscopic or subnanoscopic corrugations, in conditions close to coexistence, vapor nucleation is typically characterized by large free energy barriers, of tens to hundreds of k_BT. Thus, similar to the homogeneous or heterogeneous case, nucleation within surface textures cannot be investigated by *brute force* MD or MC simulations. To this purpose, advanced sampling techniques for rare events have been used, including US and FFS explained in Sec. II, restrained MD (RMD[53]), and Boxed dynamics (BXD[54]). In addition to the nucleation rate and/or the free energy profile, these methods allow one to gather insights into the nucleation path. Indeed, US, RMD, and BXD are all methods for computing conditional averages; therefore, with these techniques, it is possible to characterize the nucleation process via conditional averages of suitable observables such as the density field. This approach has been applied to nucleation in slit pores,[55] isolated (essentially) 2D grooves,[28,38,40,56,57] and interconnected pillared structures.[31] In all these studies, the observable used to accelerate the process is the number density in a region of space containing the corrugations. In a liquid-vapor system, this observable is equivalent to the vapor (or liquid) volume in the same spatial domain, i.e., the observable used in CNT and its extensions. The nucleation path is analyzed by computing the instantaneous[58] or the average liquid-vapor interface, corresponding to a suitable isosurface of the density field. Examples of these paths for 2D and 3D corrugations are

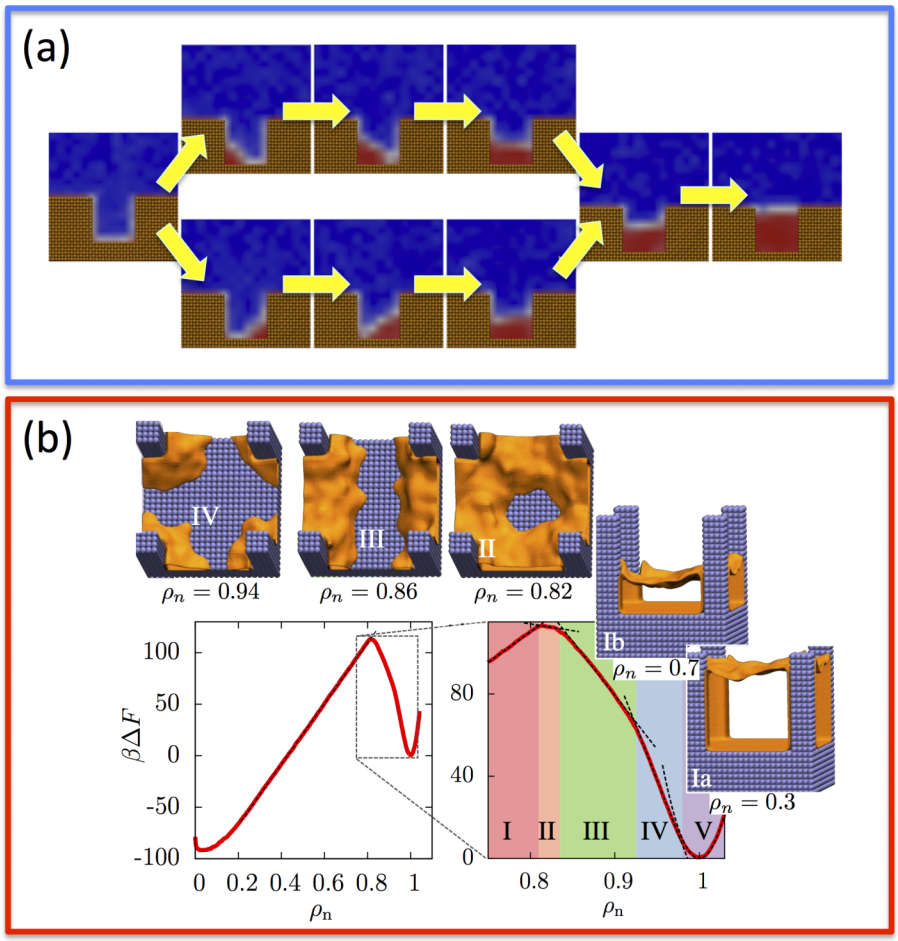

FIG. 10. Nucleation path of a vapor bubble (a) in a 2D rectangular pore and (b) in a 3D pillared structure. For the 3D surface, it is also reported for the free energy profile going from $\rho_n = 0$, vapor in the pore, to $\rho_n = 1$, liquid in the pore. An enlarged view of the initial part of the nucleation path is also shown highlighting the effect of the discontinuities on the profile. Panel (a) adapted with permission from Giacomello *et al.*, Langmuir **28**, 10764 (2012). Copyright 2012 American Chemical Society. Panel (b) adapted with permission from S. Prakash, E. Xi, and A. J. Patel, Proc. Natl. Acad. Sci. U. S. A. **113**, 5508 (2016). Copyright 2016 Authors.

illustrated in Fig. 10 (see also Refs. 40, 56, and 57 for more complicated re-entrant structures). A common trait of these paths is that they are composed of branches with different morphologies of the liquid-vapor interface. As for the macroscopic cases discussed in Sec. IV, discontinuities in the nucleation path, corresponding to morphological transitions, indicate a (local) insufficiency of the single order parameter used for describing nucleation.

The string method in collective variables[59] overcomes the limitations of the previous approaches, yielding the most likely (continuous) path in the limit of an infinitely long duration of the transition process. At a variance with US, RMD, and BXD, the string method enforces the continuity of the path; in addition, it can be used in conjunction with a large number of order parameters. References 30 and 48 show that the actual vapor nucleation path in isolated and interconnected textured surfaces is different from those identified by RMD and US. An example of such a path for a 2D case is shown in Fig. 11(a). Indeed, the departure of RMD from the actual (string) path is limited to a narrow region close to the morphological transition. However, this might have significant consequences on the estimation of the free energy barrier, of the order of 20%.[30]

The departure from the actual nucleation path is more significant in the case of surfaces with interconnected textures. In the case of US simulations,[31] the nucleation path proceeds *via* a number of well-defined liquid-vapor interface morphologies (Fig. 11(b)). String simulations, however, reveal that the nucleation path is much more complex and involves multiple length scales. The process starts with the formation of two low-density regions at the base of two facing pillars (Fig. 11(b)). These regions grow and merge into a continuous depleted region between the pillars. This domain then percolates to neighboring pillars, forming a connected vapor network. The vapor then starts to form also in the domains among four pillars and detaches from the bottom forming a proper bubble with a fully formed liquid-vapor interface. A liquid finger eventually detaches from the bottom of the surface, in a point between two pillars; this configuration corresponds to the transition state. The reader is warned that there are minor differences between the systems shown in Figs. 10(b) and 11(b), e.g., the liquid model is SPC/E[60] water in the first case and LJ in the other. However, we believe that the main difference between the two paths actually lies in the different simulation techniques used to explore the complex free energy landscape of vapor nucleation at pillared surfaces.

Also in the case of 3D pillared structure, US/RMD provides wrong estimation of the barrier.[48] An intuitive reason for this error can be drawn in the limit of low temperature. In this case, in *pure* US and RMD simulations, the system moves along the "valleys" of the free energy, exploring only those microstates whose energy falls within few k_BT from the bottom of the valley at the current value of the observable

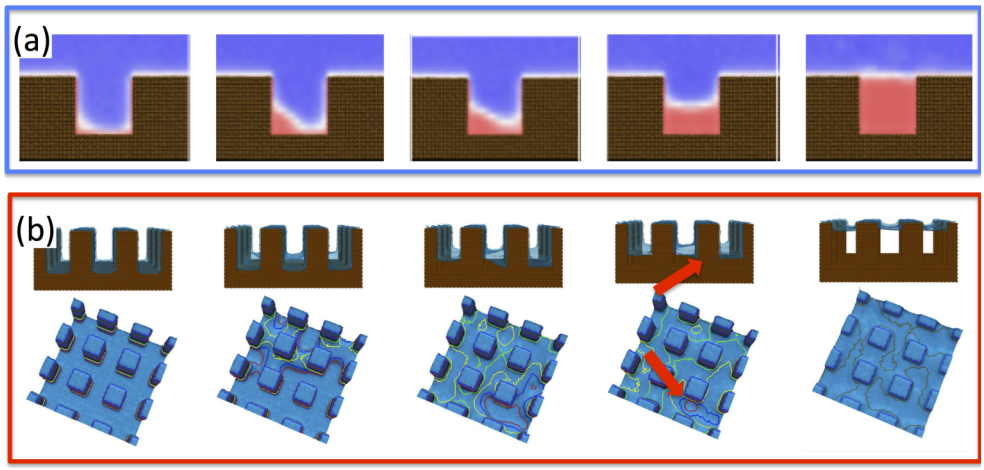

FIG. 11. Nucleation paths obtained *via* the string method (a) for a 2D groove and (b) for a 3D pillared surface. In the panel (b), to help the reader to identify the position of the meniscus, the contour lines of the liquid/vapor/solid triple line are colored according to their level: red close to the bottom, blue close to the top of the surface. The red arrows point to the liquid finger in between pillars mentioned in the main text. Both geometries are similar to those in Fig. 10. Panel (a) Reproduced with permission from J. Chem. Phys. **142**, 104701 (2015). Copyright 2015 AIP Publishing LLC.

used for the biasing (the number density in the case of the article cited above). Thus, the transition from one morphology to the other takes place only when the barrier in a direction orthogonal to the biasing observable is of the order of k_BT. The actual (lower) energy barrier might be placed before this point (see also Ref. 61). Indeed, in the presence of multiple conditional metastabilities separated by large barriers, *pure* US/RMD simulations may yield an incorrect estimate of the free energy of the single collective variable. In extreme cases this might bring to missing the presence of genuine stable and metastable states.

To better explain these effects, consider the sketch of a two-dimensional free energy surface in Fig. 12(a). Here, both degrees of freedom are necessary to characterize the metastabilities and transition path. The black dashed and dotted lines denote the paths typically followed in *pure*,

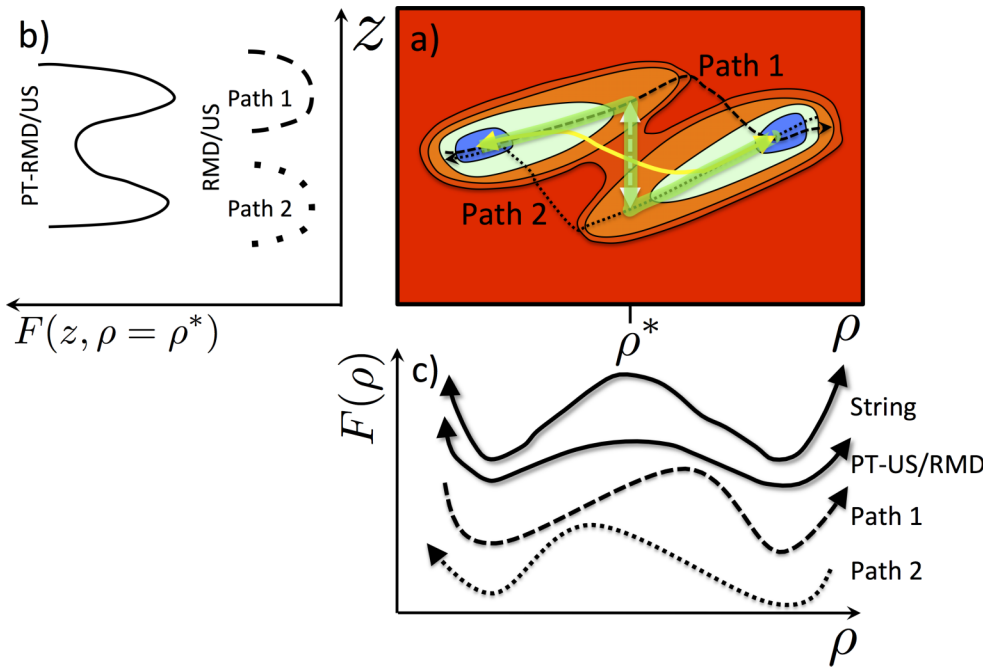

FIG. 12. (a) Sketch of a two-dimensional free energy surface. In this example, both degrees of freedom are necessary to characterize the metastabilities and transition path. The marginalization of the joint probability, i.e., the integration of one of the two variables, associated to this two-dimensional free energy yields the free energy of ρ, $F(\rho) = -k_BT \log \int dz \exp[-F(z,\rho)/(k_BT)]$. This marginalization is implicitly performed by RMD/US. However, in the presence of large free energy barriers in orthogonal directions, i.e., along any of the variables that are marginalized, like in the example of this panel, pure RMD/US cannot properly compute $F(\rho)$. (b) Free energy profile along the second degree of freedom, z, at a prescribed value of ρ, $\rho = \rho^*$ as obtained from pure RMD/US along the paths 1 and 2, and with PT-RMD/US. (c) Cartoons of free energy profiles obtained from pure RMD/US started from either minima and PT-RMD/US. A cartoon of the free energy profile obtained from a string calculation and projected on the single variable ρ is also reported. In all plots, the sketches of the free energy profiles are shifted to improve readability, only relative values within the curves matter. Adapted with permission from S. Orlandini, S. Meloni, and G. Ciccotti, J. Stat. Phys. **145**, 812 (2011). Copyright 2011 Springer.

low-temperature US/RMD simulations biased along the ρ variable starting the process from either minimum. Fig. 12(b) shows the free energy profiles along the second degree of freedom, z, at a prescribed value of ρ as obtained from *pure* US/RMD simulations started from the two minima. Panel (c) of the same figure presents the corresponding profiles of free energy; the profiles differ between them, showing a sizable hysteresis. This problem can be solved by combining RMD/US with parallel tempering[62] (PT). In the simplified example of Fig. 12(a), the PT-RMD/US path is the combination of the dashed and dotted branches departing from the respective minima, which switch basin in correspondence with the white dashed line with two arrows (path highlighted in green). The transition between the two valleys occurs when the *local* free energy at the same value of ρ in the two basins is the same. This transition anticipates the one observed in pure, low-temperature RMD/US simulations. The free energy profile of the PT-RMD/US path is reported in Fig. 12(c); the comparison with the profiles of *pure* RMD/US shows that the PT-RMD/US barrier is lower. PT-RMD has been shown to be effective in sampling of the space orthogonal to the chosen nucleation variable in the related order-disorder phase transitions.[63]

However, also PT-US/RMD is insufficient to accurately estimate the barrier. Indeed, with PT-US/RMD the barrier is underestimated because along the residual slow degrees of freedom, the system is located within few k_BT of the minimum at the given value of the biasing observable, rather than at the saddle point of the overall system. This can be understood considering the free energy profile along the second degree of freedom at a prescribed value of ρ shown in Fig. 12(b). The string method allows one to overcome these limitations. Although computationally more expensive than PT-US/RMD, its cost scales only linearly with the number of degrees of freedom, allowing feasible computations of relatively complex systems.[48]

VIII. KINETIC AND INERTIAL EFFECTS

This section is relative to panel (D.2) of Fig. 2.

In Secs. II–VII we have considered the *mean field* effects of the interface between a liquid and its vapor and between a fluid and a solid. At finite temperature, the interface, whether atomistic or macroscopic, undergoes fluctuations which may have an effect on the nucleation path. In addition, the results discussed so far are obtained within the quasi-static approximation, which has two types of implications: (i) the nucleation trajectory takes an infinite time; (ii) along the trajectory, the system reaches the conditional equilibrium at each value of the observable controlling the nucleation. In this section we will discuss some of the attempts made to go beyond these limitations, to investigate kinetic effects; the main challenge here is the need of obtaining unbiased trajectories, which are computationally unaffordable in the presence of the large barriers typical of nucleation. Indeed, few rare event techniques are capable of sampling unbiased trajectories; among those, the FFS mentioned above and the transition path sampling[61] (TPS). However, apart from few studies,[17,23,46,64] to date such methods have not been extensively applied to vapor nucleation in confined systems.

Other approaches that have been considered for investigating the contribution of kinetic effects on nucleation are based on coarse grained models of the fluid. This approach mitigates the problem of rare events by increasing the shortest time scale from the atomic to the *mesoscopic* one, or the corresponding collective MC move. In this context, Lum and Luzar[65] made an early attempt to study vapor nucleation in confined geometries, namely, in a liquid confined between two finite hydrophobic walls. Their simulations are based on the lattice-gas model of a fluid and its vapor, with the system described by the Hamiltonian

$$H(\{n_i\}_{i=1,N}) = -\epsilon \sum_{i,j} n_i n_j - \sum_{i \in \text{surface}} \epsilon_i^s n_i - \mu \sum_i n_i. \qquad (9)$$

Here, n_i denotes the state of a grid point in the discretization of the space; $n_i = 0$ for vapor and $n_i = 1$ for liquid. The first sum runs over nearest neighbor pairs, and ϵ is the associated interaction. The second sum runs over *surface sites*, and ϵ_i^s is the corresponding fluid-surface interaction. Finally, μ is the difference of chemical potential between the vapor and the liquid. *Glauber dynamics*, consisting of a MC trajectory in which the state of individual sites is changed (no mass conservation), is performed to investigate the nucleation mechanism. The simulation is prepared such that the space between hydrophobic walls is initially filled with liquid, which is metastable in the simulated conditions. Very quickly a vapor layer forms at the walls, while the newly formed liquid-vapor interface undergoes long wavelength thermal fluctuations. The excitation of fluctuations with a shorter wavelength eventually brings in contact the liquid-vapor interfaces at the top and bottom walls. A cavity connecting the two walls is thus formed. This cavity can recede, bringing back the system to the initial metastable liquid state, or proceed towards total evaporation. A general conclusion drawn by the authors is that "[...] the evaporation pathway cannot be fully captured with interfacial models in which short wavelength fluctuations are integrated out." While this conclusion points to intriguing kinetic effects which have not received enough attention to date, they seem partially in conflict with the later results of Sharma and Debenedetti mentioned above,[46] who found good agreement between the nucleation barrier calculated via sharp interface and atomistic models of a fluid. Indeed, several authors (see, e.g., Refs. 38, 30, and 55) have shown that to a large extent, interface models can support curvatures corresponding to the short wavelength modes.

Quasi-static nucleation models in general, including those based on sharp and diffuse interfaces, as well as those derived from atomistic simulations, assume a time scale separation between the slow variables describing the transition and the remaining ones. However, several *in silico* experiments have shown that this assumption is not always satisfied. Moreover, quasi-static models neglect inertial effects, i.e., the departure from the ideal path in the free energy landscape when the process takes place at finite speed. An example of the possible effects of fluctuations in homogeneous vapor nucleation is provided in Ref. 17; there the local departure of the temperature from the equilibrium value is found to trigger nucleation. For homogeneous nucleation, quasi-static results

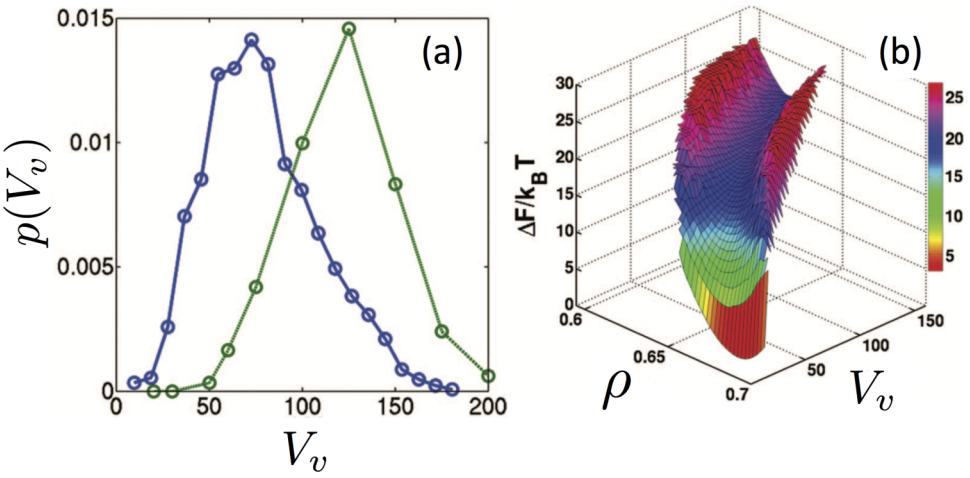

FIG. 13. (a) Distribution of bubble volumes at the system density corresponding to the BXD (blue circles) and FFS (green circles) transition states. (b) Free energy landscape of nucleation in the stretched LJ fluid as a function of the reduced density of the simulation box, ρ, and the bubble volume, V_v. Reproduced with permission from J. Chem. Phys. **137**, 074109 (2012). Copyright 2012 AIP Publishing LLC.

from US and BXD have been compared with dynamical approaches, FFS in the present case.[23] The results of this work suggest that in the simulated conditions, there are no important kinetic or inertial contributions to the vapor nucleation mechanism. The main difference between quasi-static and FFS approaches is the distribution of the vapor bubbles at the thermodynamic (maximum of the free energy) and kinetic (50% probability that trajectories reach the vapor state) transition states (Fig. 13(a)). The minor importance of kinetic effects is probably related to the relatively simple free energy landscape of homogeneous nucleation in a small sample (~3000 particles) far from spinodal conditions (Fig. 13(b)). Closer to spinodal conditions or, depending on the thermodynamic conditions, in larger samples, it is possible that the liquid-to-vapor transition proceeds via the formation, coalescence, and growth of multiple bubbles. In these conditions, a more complicated free energy landscape governs the process, and kinetic and inertial effects might become more important.

The faster is the transition, the more finite time effects are expected to play a role. These effects can be thoroughly investigated via the minimum action method[66] (MAM), which yields the most probable transition path connecting the initial and final states in a prescribed time interval. In the original article, this approach is applied to a model problem of interest for nucleation phenomena, namely, the thermally activated switching of a bistable system modeled by the Ginzburg-Landau equation; this problem can be interpreted as the evolution of the interface between two phases. The system, described by a 1D density field $\rho(x,t)$, is characterized by two metastable states of high and low density at coexistence, designated as ρ_I and ρ_{II}, respectively. MAM allowed the authors to investigate the dependence of the transition path on the duration of the process. It is shown that for a slow process, the phase transition takes place *via* the formation of a single nucleus (Fig. 14), with the path passing through (close) the transition state of minimum energy; this is similar to what would happen in the quasi-static limit. On the contrary, if the trajectory is faster, the phase transition follows paths characterized by more nuclei, with an associated higher barrier which is consistent with the increased number of interfaces.

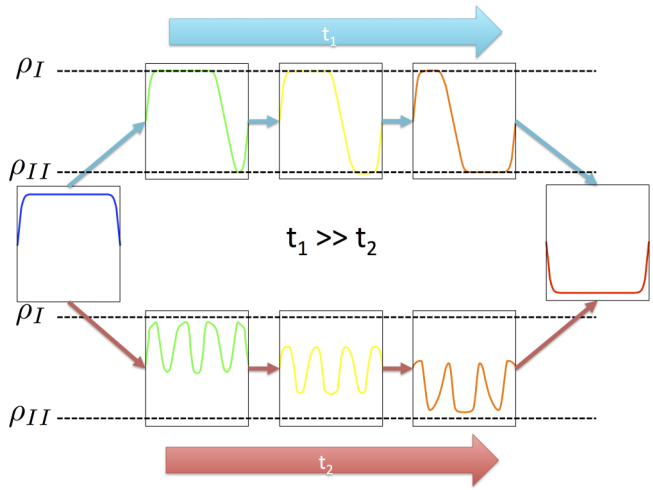

FIG. 14. Evolution of the interface between the coexisting phases ρ_I and ρ_{II}, for two different durations of the transition, $t_1 \gg t_2$. The value of the density field is constrained to be 0 at the borders of the domain. When the process is slow, the transition proceeds by forming a single nucleus. The transition state corresponding to this path has minimum energy. For shorter durations, the system passes through other transition states with higher energies. Adapted with permission from W. E, W. Q. Ren, and E. Vanden-Eijnden, Commun. Pure Appl. Math. **57**, 637 (2004). Copyright 2004 John Wiley & Sons, Inc.

IX. CONCLUSIONS AND OUTLOOK

In this focus article, we have considered theories and computer simulations of nucleation of vapor in confined systems and at textured surfaces. We started from the classical nucleation theory in the bulk and its extension to simple heterogeneous systems. We have then introduced the *continuum rare events method* — CREaM — which extends CNT to complex confined systems. CNT and CREaM are based on the same set of hypotheses, i.e., (i) the multiphase fluid is described by a sharp interface model, (ii) nucleation follows a quasi-static path, and (iii) the transition can be *monitored* through a single observable, namely, the volume of the vapor domain. Although these simpler models provide the correct qualitative picture in most of the cases, there are conditions where they fail to accurately describe the nucleation process. We have presented and discussed more

complete formulations that go beyond the limitations of classical approaches. The non-classical effects have also been reviewed, with special emphasis on models of vapor nucleation in confined systems and textured surfaces.

Capturing all these, sometimes subtle, effects, can be computationally unaffordable especially in complex environments. A challenge for the field is therefore identifying the conditions in which simple and inexpensive models, such as CNT, work well and when it is instead crucial to use a more accurate description of the phenomenon. Indeed, the computational cost grows significantly with the complexity of the fluid model and the computational technique adopted to identify the nucleation path. The result is that, presently, a better description of nucleation can only be achieved at the cost of studying relatively small systems. To the best of our knowledge, the largest simulation of vapor nucleation in a pillared surface involved a 3×3 pillar structure, for a total of ~200 000 particles (Fig. 11(b)). However, this kind of simulations cannot be performed routinely these days, and many real-life problems require much bigger samples. For example, early simulations of vapor nucleation in a hydrophobic slit pore with hydrophilic patches with regular or random distribution have revealed a rich phenomenology.[67] It would be interesting to check whether the relatively simple principles identified for the slit pore case are also valid for actual natural surfaces. These latter surfaces are often characterized by very complex chemistry and topography (see, for example, the surface of the Salvinia molesta fern[68]) and their simulation requires much bigger samples, which is presently out of reach for the most advanced methods (atomistic simulations). It can be thought of attacking such problems by using a hierarchy of techniques, with the more sophisticated and computationally expensive techniques providing input parameters for the simpler and computationally more affordable. Another approach consists in developing genuine multi-scale techniques, with the various levels of description of the multiphase system cooperating together (see, e.g., Ref. 69 and references therein).

Instrumental to both approaches is the extension of techniques for rare events to the domain of continuum physics. So far there have been just few attempts in this direction, e.g., using the sharp interface model together with conditional minimization[29] or combining a DFT model of the fluid with the nudged elastic band (see Ref. 70 and the review article Ref. 71) or with the string method.[72] Other powerful techniques, such as FFS, could in principle also be extended to the continuum description of fluids, e.g., in combination with fluctuating hydrodynamics[73] to investigate vapor nucleation with kinetic and inertial effects at a continuum level. This seems a very promising direction for investigating vapor and gas nucleation on time and length scales of technological relevance.

Summarizing, despite the enormous progress of research in gas/vapor nucleation during the last couple of decades, many fundamental physical aspects and their application to chemistry and engineering remain elusive. In particular, given the strong sensitivity of nucleation to the environmental conditions, there is a lack of reliable quantitative results, both computational and experimental, against which nucleation theories can be validated. We hope that these challenges will encourage methodological developments of atomistic and continuum computer simulations and, at the same time, will stimulate quantitatively reliable experiments of vapor nucleation in controlled conditions.

ACKNOWLEDGMENTS

The authors acknowledge fruitful discussion with Matteo Amabili, Antonio Tinti, Emanuele Lisi, and Sara Marchio. The research leading to these results has received funding from the European Research Council under the European Union's Seventh Framework Programme (No. FP7/2007-2013)/ERC Grant Agreement [No. 339446].

[1]V. K. Dhir, Annu. Rev. Fluid Mech. **30**, 365 (1998).
[2]K. S. Suslick, Science **247**, 1439 (1990).
[3]C. E. Brennen, *Cavitation and Bubble Dynamics* (Cambridge University Press, New York, 2014).
[4]V. P. Skripov, *Metastable Liquids* (Halsted Press, 1972).
[5]R. N. Wenzel, Ind. Eng. Chem. **28**, 988 (1936).
[6]A. B. D. Cassie and S. Baxter, Trans. Faraday Soc. **40**, 546 (1944).
[7]W. Barthlott and C. Neinhuis, Planta **202**, 1 (1997).
[8]The tilting angle is the inclination of a surface sufficient to make droplets roll along it. Superhydrophobic surfaces have low tilting angles.
[9]S. T. Yohe, Y. L. Colson, and M. W. Grinstaff, J. Am. Chem. Soc. **134**, 2016 (2012).
[10]R. Carlisle, J. Choi, M. Bazan-Peregrino, R. Laga, V. Subr, L. Kostka, K. Ulbrich, C. C. Coussios, and L. W. Seymour, J Natl Cancer I **105**, 1701 (2013).
[11]J. J. Kwan, R. Myers, C. M. Coviello, S. M. Graham, A. R. Shah, E. Stride, R. C. Carlisle, and C. C. Coussios, Small **11**, 5305 (2015).
[12]O. Pedersen and T. D. Colmer, J. Exp. Biol. **215**, 705 (2012).
[13]N. J. Shirtcliffe, G. McHale, M. I. Newton, C. C. Perry, and F. B. Pyatt, Appl. Phys. Lett. **89**, 104106 (2006).
[14]K. F. Kelton and A. L. Greer, *Nucleation in Condensed Matter: Applications in Materials and Biology* (Pergamon, 2010).
[15]R. P. Sear, J. Phys.: Condens. Matter **19**, 033101 (2007).
[16]V. K. Shen and P. G. Debenedetti, J. Chem. Phys. **111**, 3581 (1999).
[17]Z.-J. Wang, C. Valeriani, and D. Frenkel, J. Phys. Chem. B **113**, 3776 (2009).
[18]G. M. Torrie and J. P. Valleau, J. Comput. Phys. **23**, 187 (1977).
[19]More in general, US allows to compute the *Landau* thermodynamic potential consistent with the conditions of the simulation.
[20]Different implementations of the LJ potential, e.g., cutoffs and/or shifting procedures (force shifting *vs* potential shifting), might result in different phase diagrams. Thus, the same nominal value of pressure and temperature may correspond to different points in the phase diagram of the two systems, namely, different values of supersaturation.
[21]R. J. Allen, P. B. Warren, and P. R. ten Wolde, Phys. Rev. Lett. **94**, 018104 (2005).
[22]P. R. ten Wolde, M. J. Ruiz Montero, and D. Frenkel, Faraday Discuss. **104**, 93 (1996).
[23]S. L. Meadley and F. A. Escobedo, J. Chem. Phys. **137**, 074109 (2012).
[24]J. Diemand, R. Angélil, K. K. Tanaka, and H. Tanaka, Phys. Rev. E **90**, 052407 (2014).
[25]E. Ruckenstein and Y. Djikaev, Adv. Colloid Interface Sci. **118**, 51 (2005).
[26]E. Ruckenstein and G. Berim, *Kinetic Theory of Nucleation* (CRC Press, Boca Raton, FL, USA, 2016).
[27]V. K. Shen and P. G. Debenedetti, J. Chem. Phys. **118**, 768 (2003).
[28]A. Giacomello, S. Meloni, M. Chinappi, and C. M. Casciola, Langmuir **28**, 10764 (2012).
[29]A. Giacomello, M. Chinappi, S. Meloni, and C. M. Casciola, Phys. Rev. Lett. **109**, 226102 (2012).
[30]A. Giacomello, S. Meloni, M. Müller, and C. M. Casciola, J. Chem. Phys. **142**, 104701 (2015).
[31]S. Prakash, E. Xi, and A. J. Patel, Proc. Natl. Acad. Sci. U. S. A. **113**, 5508 (2016).
[32]N. A. Patankar, Langmuir **20**, 7097 (2004).
[33]M. Nosonovsky and B. Bhushan, Microsyst. Technol. **12**, 231 (2006).
[34]Q. S. Zheng, Y. Yu, and Z. H. Zhao, Langmuir **21**, 12207 (2005).
[35]Y. Su, B. Ji, K. Zhang, H. Gao, Y. Huang, and K. Hwang, Langmuir **26**, 4984 (2010).

[36]P. Lv, Y. Xue, H. Liu, Y. Shi, P. Xi, H. Lin, and H. Duan, Langmuir **31**, 1248 (2014).
[37]A. Page and R. Sear, Phys. Rev. Lett. **97**, 065701 (2006).
[38]A. Giacomello, M. Chinappi, S. Meloni, and C. M. Casciola, Langmuir **29**, 14873 (2013).
[39]K. A. Brakke, Exp. Math. **1**, 141 (1992).
[40]M. Amabili, E. Lisi, A. Giacomello, and C. M. Casciola, Soft Matter **12**, 3046 (2016).
[41]D. W. Oxtoby and R. Evans, J. Chem. Phys. **89**, 7521 (1988).
[42]G. Navascues and P. Tarazona, J. Chem. Phys. **75**, 2441 (1981).
[43]V. Talanquer and D. W. Oxtoby, J. Chem. Phys. **104**, 1483 (1996).
[44]L. Schimmele, M. Napiórkowski, and S. Dietrich, J. Chem. Phys. **127**, 164715 (2007).
[45]L. Schimmele and S. Dietrich, Eur. Phys. J. E **30**, 427 (2009).
[46]S. Sharma and P. G. Debenedetti, Proc. Natl. Acad. Sci. U. S. A. **109**, 4365 (2012).
[47]L. Guillemot, T. Biben, A. Galarneau, G. Vigier, and E. Charlaix, Proc. Natl. Acad. Sci. U. S. A. **109**, 19557 (2012).
[48]M. Amabili, A. Giacomello, S. Meloni, and C. M. Casciola, "Collapse of superhydrophobicity on nanopillared surfaces" (unpublished).
[49]F. Dell'Isola, H. Gouin, and P. Seppecher, CR Acad Sci II B-Mec **320**, 211 (1995).
[50]V. Talanquer and D. W. Oxtoby, J. Chem. Phys. **114**, 2793 (2001).
[51]DFT has also been combined with the Nudged Elastic Band[74] method to compute the entire nucleation path.[70]
[52]Y. Liu, Y. Men, and X. Zhang, J. Chem. Phys. **137**, 104701 (2012).
[53]L. Maragliano and E. Vanden-Eijnden, Chem. Phys. Lett. **426**, 168 (2006).
[54]D. R. Glowacki, E. Paci, and D. V. Shalashilin, J. Phys. Chem. B **113**, 16603 (2009).
[55]R. C. Remsing, E. Xi, S. Vembanur, S. Sharma, P. G. Debenedetti, S. Garde, and A. J. Patel, Proc. Natl. Acad. Sci. U. S. A. **112**, 8181 (2015).
[56]E. S. Savoy and F. A. Escobedo, Langmuir **28**, 16080 (2012).
[57]M. Amabili, A. Giacomello, S. Meloni, and C. M. Casciola, Adv. Mater. Interfaces **2**, 1500248 (2015).
[58]A. P. Willard and D. Chandler, J. Phys. Chem. B **114**, 1954 (2010).
[59]L. Maragliano, A. Fischer, E. Vanden-Eijnden, and G. Ciccotti, J. Chem. Phys. **125**, 024106 (2006).
[60]H. J. C. Berendsen, J. R. Grigera, and T. P. Straatsma, J. Phys. Chem. **91**, 6269 (1987).
[61]P. G. Bolhuis, D. Chandler, C. Dellago, and P. L. Geissler, Annu. Rev. Phys. Chem. **53**, 291 (2002).
[62]R. H. Swendsen and J.-S. Wang, Phys. Rev. Lett. **57**, 2607 (1986).
[63]S. Orlandini, S. Meloni, and G. Ciccotti, J. Stat. Phys. **145**, 812 (2011).
[64]E. S. Savoy and F. A. Escobedo, Langmuir **28**, 3412 (2012).
[65]K. Lum and A. Luzar, Phys. Rev. E **56**, R6283 (1997).
[66]W. E, W. Q. Ren, and E. Vanden-Eijnden, Commun. Pure Appl. Math. **57**, 637 (2004).
[67]K. Leung and A. Luzar, J. Chem. Phys. **113**, 5836 (2000).
[68]W. Barthlott, T. Schimmel, S. Wiersch, K. Koch, M. Brede, M. Barczewski, S. Walheim, A. Weis, A. Kaltenmaier, A. Leder, and H. F. Bohn, Adv. Mater. **22**, 2325 (2010).
[69]M. K. Matthew K. Borg, D. A. Lockerby, and J. M. Reese, J. Fluid Mech. **768**, 388 (2015).
[70]J. F. Lutsko, J. Chem. Phys. **129**, 244501 (2008).
[71]H. Kusumaatmaja, J. Chem. Phys. **142**, 124112 (2015).
[72]A. Giacomello, L. Schimmele, and S. Dietrich, Proc. Natl. Acad. Sci. U. S. A. **113**, E262 (2016).
[73]J. M. Ortiz de Zárate and J. V. Sengers, *Hydrodynamics Fluctuations in Fluids and Fluid Mixtures* (Elsevier, 2006).
[74]H. Jónsson, G. Mills, and K. W. Jacobsen, in *Classical and Quantum Dynamics in Condensed Phase Simulations*, edited by B. J. Berne, G. Ciccotti, and D. F. Coker (World Scientific, Singapore, 1998), p. 385.